

TIANWEN LI *

OPEN PIT MINE INTEGRATING YOLO OPTIMIZATION MODEL AND TRIANGULATION NETWORK STOPE DATA EXTRACTION METHOD

To achieve the automatic, rapid, and precise extraction of stope data from open-pit mines, this paper introduces a novel stope data extraction method based on an enhanced Mine-YOLO model integrated with a triangulated network. An attention mechanism is incorporated to improve the capture of channel, spatial, and global multi-scale features, enabling the model to effectively consider both global context and boundary details of open-pit stopes while enhancing its ability to distinguish positive samples through an optimized loss function. Following dataset training and validation, the average accuracy for stope identification and segmentation using the Mine-YOLO model has improved by 0.15 and 0.079 respectively compared to the baseline model. The Mine-YOLO framework is employed to extract stope areas from DEM data; subsequently, indices such as stope area, volume, and mining depth are automatically calculated via a constructed triangulation network. The average errors in extracted stope area, volume, and mining depth are found to be 0.058, 0.047, and 0.002 respectively – demonstrating that the proposed methodology possesses high accuracy and significant practical application value.

Keywords: Improved YOLOv8; Spatial attention mechanism; Extraction from open pit mine; TIN triangle network; Image segmentation Subject classification codes: temporarily no

1. Introduction

Open-pit mining occupies a major position in mineral mining, with higher efficiency and output compared with underground mining, and has become the economic pillar of a country and a region. However, due to the long-term and dynamic nature of open-pit mining, as well as the continuous updating of mining technology and equipment, and driven by economic interests, bad behaviors such as theft, illegal mining and disorderly mining of mineral resources occur from time to time, the high-intensity mining of mineral resources in mining cities has brought new

¹ YANGTZE UNIVERSITY, SCHOOL OF GEOSCIENCES, WUHAN 430074, CHINA

* Corresponding author: 3258174500@qq.com



environmental challenges and regulatory difficulties. Therefore, in open pit mining, regular and continuous access to open pit stope information is of great significance for miners to formulate and modify production plans, for environmental supervision departments to evaluate the impact of mining on the environment, and for resource management departments to monitor mining dynamics and prevent ultra-deep and ultra-range mining [1]. The traditional method of obtaining information in open pit mine needs field survey and costs manpower and material resources. With the rapid development of remote sensing technology, and due to the complex terrain of open-pit mines, remote sensing, as a non-invasive monitoring method, is the most widely used and effective among many open-pit monitoring methods [2]. In particular, the application of UAV aerial survey technology provides a new means for accurate and efficient acquisition of open-pit mine data [3]. The images taken by the open-pit mine UAV and the DEM data generated by the subsequent photogrammetric processing provide data support for this task [4].

However, the original remote sensing images of open pit mines were all identified and extracted by experts using visual interpretation, which is subjective and costly. Later, more and more researchers tried to find methods for automatic or semi-automatic classification and extraction of remote sensing images [5-7]. Balaniuk et al. (2020) used CNN model and sentinel-2 satellite data to identify tailings DAMS in mining areas [8]. Xie et al. (2020) used GaoFen-2 satellite images to create semantic segmentation data sets for open pit mines through manual annotation, and proposed a pixel-level semantic segmentation model based on U-Net [9]. Chen et al. (2021) proposed an improved U-Net+ multi-layer feature association deep learning network to reduce feature loss in open-pit mines by ensuring the maximum value of feature mappings in each layer of the network [10]. However, due to the complex pattern performance and irregular spatial distribution of open pit mines, the segmentation integrity of pixel-level segmentation model is not good in complex scenes such as open pit mines. Xie et al. (2021) introduced DUsegNet, a new network used to segment open pit mines. It has the advantages of SegNet, UNet and D-LinkNet at the same time, showing better segmentation ability of solid objects on GaoFen-2 images [11]. Liu et al. (2023) proposed an end-to-end small object detection and driveable area segmentation framework for open surface mining, aiming at the dense density and blurred boundaries of small objects on unstructured roads in mining scenarios. This framework combined lightweight attention modules to enhance the attention to the space and channel dimensions of small objects without slowing down the reasoning speed [12]. Men et al. (2024) proposed a gleaning-injection-sensing network (GIPNet) to save information from multi-scale feature fusion, improve the ability to identify and locate the boundaries of open-pit mining areas, and improve mining efficiency [13]; Guo Dongliang et al proposed to improve the lightweight PAM-M-YOLO model for image detection of coal gangue in mining areas [14]. Ruan Shunling et al. (2024) explored a new method to detect negative obstacles in roads of opencore mines. In this method, BiFPN feature fusion module is used to improve the detection weight ratio of small negative obstacles, and dual attention mechanism of space and channel is introduced to enhance the feature extraction and fusion ability of the edge of negative obstacles, so as to improve the detection accuracy of small-scale negative obstacles on roads [15].

Previous studies based on deep learning provide a direction for the rapid identification and extraction of open-pit mines, but in most cases, lightweight models reduce the amount of computation and also reduce the ability of feature extraction. As a result, the extraction area boundary is larger or smaller than the target boundary, and the extraction boundary is not clear. In order to obtain accurate data of open pit stope, it is necessary to accurately extract the open pit stope boundary and improve the unity of global and local attention of the model. This paper proposes a quantitative data extraction method of open pit stope to cope with the increasingly accurate

and rapid monitoring of open pit. Explore an improved Mine-YOLO lightweight network model based on YOLOv8 network model. Add GAM (Global Attention Mechanism) [16] module that enhances capture channels and spatial features, and EAM (Efficient Multi-Scale Attention) [17,18] module that dynamically adaptively captures different scale features. The model can not only capture the global information of each channel at different scales, but also pay more attention to the identified target. Focaler-IoU loss function [19] is introduced. Focaler-IoU adjusts the weights of positive samples and negative samples to make the model pay more attention to the positive samples [20] that are difficult to classify, and accurately extract remote sensing images of open-pit mines. Quantitative monitoring indicators for open pit mines were established, including mining depth, mining area and mining volume. DEM data generated by low altitude remote sensing data generated by unmanned aerial vehicle based on the mask extracted from open pit Mine based on the improved Mine-YOLO network model was applied to obtain geographical coordinates and elevation data of open pit mines and buildings by affine matrix to obtain mining depth information. Using elevation coordinates to generate TIN triangulation network, more accurate mining area and mining volume information can be obtained to achieve quantitative monitoring of open pit mines, and provide favorable support for dynamic supervision and efficient production of open pit mines.

2. Construction of stope data set in open pit mine

2.1. Data source

The research data are from the production mining areas in Xiangyang City and Suizhou City in the west of Hubei Province, China (Fig. 1). Xiangyang City is close to Jiangnan Plain in the south, while there are some hilly areas in the north. Suizhou City has relatively flat terrain, mainly a part of Jiangnan Plain, with relatively gentle terrain and the Han River flowing through

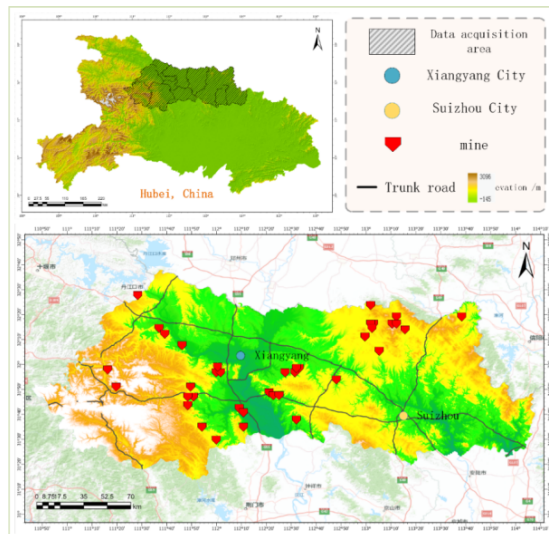


Fig. 1. Research Area

both places, with a lower elevation of 30 to 100 meters. The strata in Xiangyang and Suizhou are mainly sedimentary layers of ancient central China platform and Jiangnan Plain. The geological structure is relatively simple, and the minerals are mainly limestone, marble, sand and other minerals. Therefore, the mineral resources in the territory are mostly open-pit mining, which has a good support for the extraction and research of stope data in open-pit mines.

2.2. Method of data set construction in open pit

The research data in this paper comes from the dynamic monitoring project of open pit mines in Xiangyang City, and the data are UAV positive image data from 2022 to 2024, which mainly includes TIF image data of 39 open pit mines such as Dongjiazhuang, Hongwawuzhuang, Liyuanling, Longtanggou, Niuwei, Nanchong, Tangwangchong and Wangjiazhai. There are a total of 855 available DEM (Digital Elevation Model) image data of open pit mine. Due to the small amount of original available data, 3,100 available image data are obtained by geometric transformation processing of original image data such as rotation, cutting and image inversion. Some images are shown in Fig. 2. These transformations modify the spatial properties, orientation, and scale of the image, allowing the model to view the data from different angles and perspectives. Of these, 2170 were used for the training task of the model, 620 were used for the verification task of the model, and 310 were used for the testing task of the model.



Fig. 2. Data Image Introduction

The heterogeneity of remote sensing image collection in open-pit mines is due to the difference of data collection time and the diversity of collection environment. In order to eliminate the influence of color deviation on the performance of YOLO neural network model, some images after geometric transformation also need to be processed by color transformation. As shown in Fig. 3 below, In this paper, the brightness, saturation and contrast of images are mainly processed.

3. Comprehensive approach framework

Based on YOLOv8 network, this paper adds an attention network that enhances the capture of channel, spatial and global multi-scale features to enable the model to take into account the global and boundary details of open-pit stopes, improve the loss function to increase the model's



Fig. 3. Image transformation(cropping, color enhancement, etc.)

ability to distinguish positive samples, and make use of the original UAV images regularly obtained by regulatory authorities on open-pit mines within the jurisdiction. After processing, open pit DEM image is generated, and the generated image is enhanced with cropping and image color processing. The processed image is made into an improved Mine-YOLO for open pit stope label training, and the parameters of the training model with better accuracy are obtained, and the optimal model is used to identify and extract the open pit DEM image stope area. Based

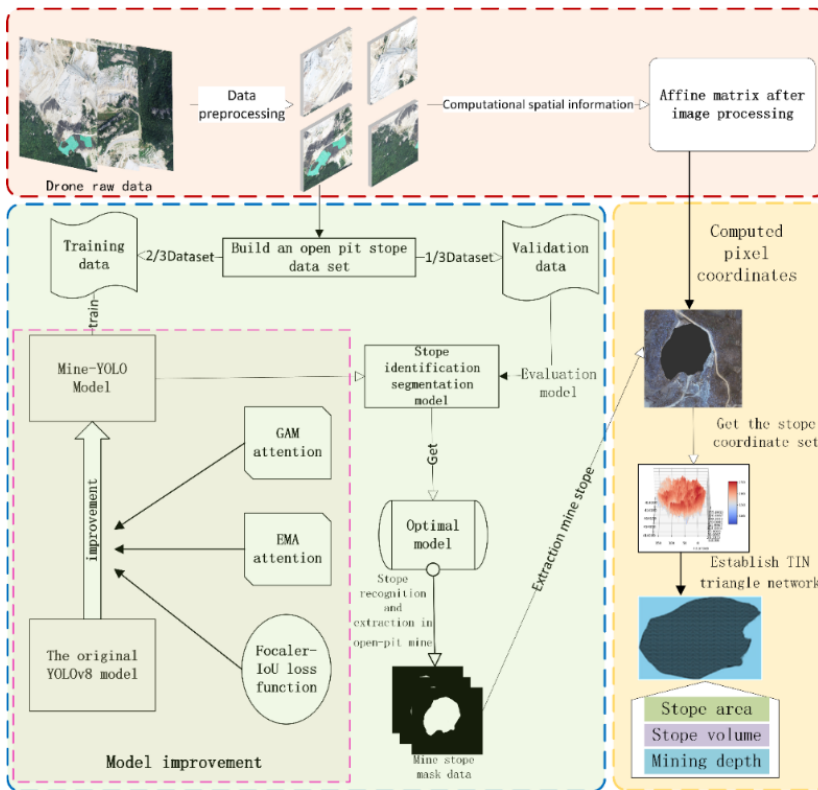


Fig. 4. Method route for obtaining quantitative data of open pit Mine based on Mine-YOLO

on the affine matrix of processing image storage, the slope area coordinate set is obtained, and a TIN (Triangulated Irregular Network) triangulation network is generated to obtain the slope area, mining volume and mining depth of the open-pit slope. The specific method flow is shown in the following figure (Fig. 4).

4. Mine-YOLO model optimization

4.1. Comprehensive architecture of the Mine-YOLO model

Based on YOLOv8 model network, this paper establishes a Mine-YOLO network model suitable for pit identification and extraction in complex environment. Since it is necessary to extract the surface slope boundary details to improve the accuracy of subsequent data, EMA (Efficient Multi-Scale Attention) multi-scale attention enhancement module is added to improve the model's identification and segmentation accuracy of mine slope boundary details. Moreover, GAM (Global Attention Mechanism) is added to retain slope feature data from the global scale to improve the accuracy of slope target identification. Replace the original loss function with Focaler-IoU (Focaler-Intersection over Union) to increase the gradient contribution of correct open-pit Mine samples to the training process. The improved Mine-YOLO model network structure is shown in the following figure (Fig. 5).

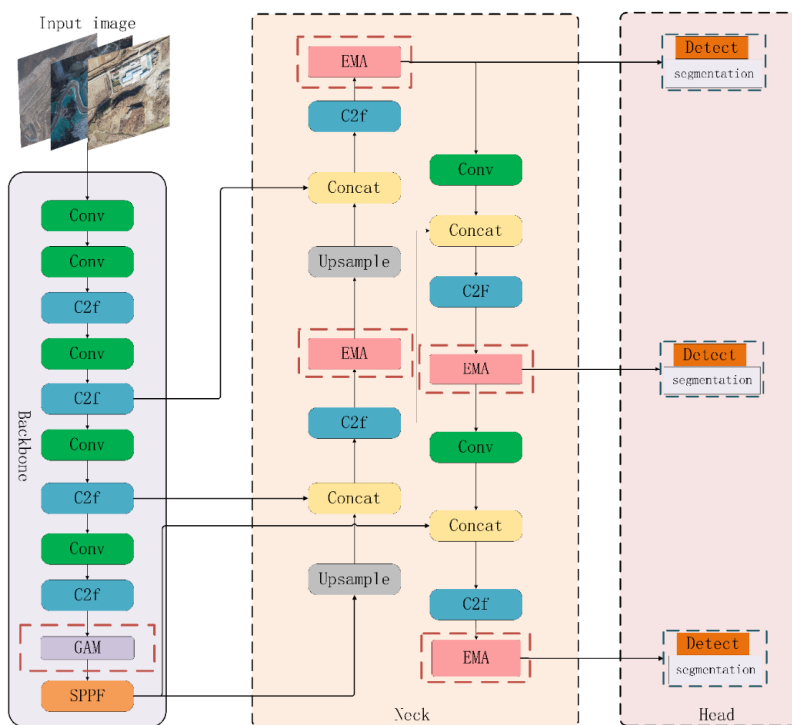


Fig. 5. Network structure of Mine-YOLO model (Red for the added attention module)

4.2. EMA Attention Module

In various computer vision tasks, channel or spatial attention mechanisms are significantly effective in generating more recognizable feature representations. However, modeling cross-channel relationships through channel dimensionality reduction may have side effects on extracting deep vision representations. Ouyang et al. proposed a novel efficient multi-scale attention (EMA) module. A new quad-space learning method is proposed, and a multi-scale parallel subnetwork is designed to deal with subfeature sets. EMA captures information at different levels by calculating attention at different scales. This method enables the model to focus on both global and local features of open-pit stopes at the same time, improving the stope capture ability in complex environments. The following figure (Fig. 6) describes the structure of EMA in detail. X Avg Pool indicates a one-dimensional horizontal global Pool, and Y Avg Pool indicates a one-dimensional vertical global pool.

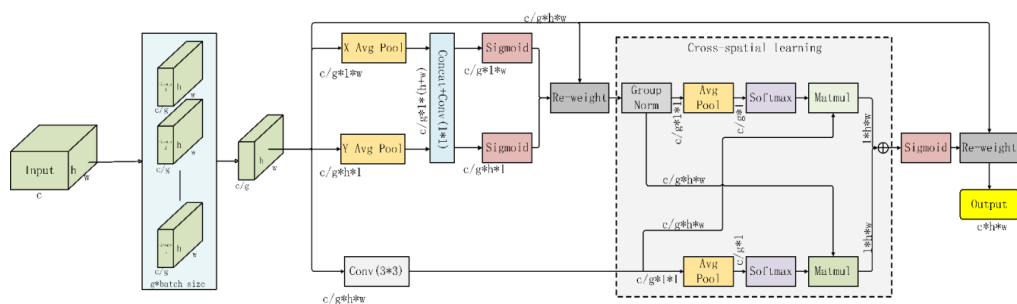


Fig. 6. EMA module network structure in Mine-YOLO

For any given input feature graph $X \in R^{c \times h \times w}$, EMA divides X into g sub-feature groups, each of which learns different semantics. This grouping approach not only enhances feature learning in the semantic region, but also compresses noise. EMA uses three parallel paths to extract the attention weights of the grouped feature maps. Two paths are 1×1 branches, and the third path is 3×3 branches. One-dimensional global averaging pooling is used in the 1×1 branch to encode channel information in two spatial directions respectively. The 3×3 branch captures multi-scale feature representations by 3×3 convolution. Specifically, the output of the 1×1 branch encodes global spatial information by two-dimensional global averaging pooling, while the output of the 3×3 branch is directly converted into the corresponding dimensional shape. These outputs are then aggregated through the matrix dot product operation to generate the first spatial attention map. Ultimately, the output feature maps within each group are aggregated by the Sigmoid function of the two generated spatial attention weight values, capturing pixel-level pairing relationships and highlighting the global context of all pixels, allowing the EMA to not only encode information across channels to adjust the importance of different channels, but also to retain precise spatial structure information into the channels. For each scale, attention is calculated separately. The final output of the EMA is the same size as the input, which makes the EMA well embedded in the YOLO model.

4.3. GAM attention module

GAM adopts the architecture of channel attention and spatial attention, and proposes a global attraction mechanism, which can enlarge the global dimensional interaction characteristics while reducing the information dispersion. GAM can better acquire the interaction between channel and space, capture important inter-dimensional information, and amplify the cross-latitude interaction. The following figure (Fig. 7) shows the network structure of GAM. Given input feature $F_1 \in R^{(c \times h \times w)}$, intermediate feature F_2 and output feature F_3 are defined by the following formulas 5 and 6:

$$F_2 = M_c(F_1) \otimes F_1 \quad (1)$$

$$F_3 = M_s(F_2) \otimes F_2 \quad (2)$$

M_c and M_s are channel attention and spatial attention respectively. \otimes represents multiplication of elements. The channel attention submodule in GAM Attention uses 3D arrangement to retain three dimensional information, amplifying cross-dimensional channel-space dependencies through a two-layer MLP (Multi-Layer perception). Its spatial attention submodule uses two convolutional layers for spatial information fusion without pooling layer, so GAM uses packet convolution for channel fusion to reduce the huge number of parameters brought by spatial attention submodule.

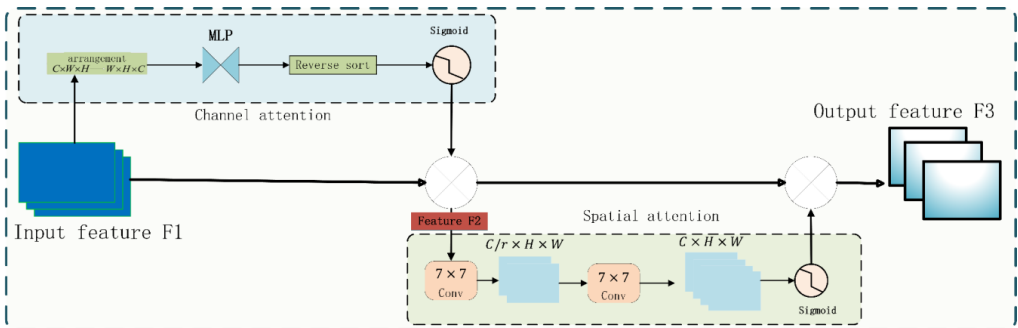


Fig. 7. GAM attention module network structure

4.4. Loss function improvement

YOLO series loss functions have been continuously improved, from Intersection over Union (IoU) to $CIoU$ (Compleat- IoU), many details have been optimized and improved. YOLOv8 adopts $CIoU$ loss function [21]. At the same time, the central-point based Anchor-Free method is introduced, and DFL (Distribution Focal Loss) is added to match Anchor-Free, so that the network can focus on the target location and the adjacent distribution area more quickly. However, since $CIoU$ itself is not sensitive to the change of the target shape, $CIoU$ is not sensitive to the change of the target shape. Moreover, due to the complexity and variety of open pit mines, the unbalance of label samples increases, resulting in poor effect of using $CIoU$ in the open pit stope identification and extraction model. Therefore, the Focaler- IoU loss function is introduced in this paper. By adjusting the weights of positive and negative samples, Focaler- IoU makes the model pay more

attention to positive samples that are difficult to classify. Thus, the weight of negative samples that are relatively easy to classify is reduced, and the ability of the model to identify rare target categories is improved [22]. The calculation expression of Focaler- IoU is as follows:

$$IoU^{focaler} = \begin{cases} 0, IoU < d \\ \frac{(IoU - d)}{u - d}, d \leq IoU \leq u \\ 1, IoU > u \end{cases} \quad (3)$$

$$L_{Focaler-IoU} = 1 - IoU^{focaler} \quad (4)$$

In the formula, $L_{Focaler-IoU}$ is the defined focaler- iOU , $IoU^{focaler}$ is the reconstructed loss calculation formula, IoU is the original IoU value, d and u are the adjustment values, so that the model can pay attention to different regression samples by adjusting the values of d and u .

5. Extraction of stope index of open pit mine

5.1. Pit index of open pit mine

According to the requirements of open-pit mine monitoring, stope information extraction is the fundamental task of this paper. According to the requirements, the quantitative data indicators of the stope shown in the following table (TABLE 1) are established. The open pit mining mineral resources in the study area are stone, marble and sand for construction. According to the DEM data of open pit Mine obtained by UAV, through the analysis of image data, combined with the improved Mine-YOLO model for identification and segmentation processing, DEM images of open pit stope area are obtained, and TIN triangle network is automatically established. Rapid acquisition of stope area, elevation volume, mining depth quantitative data.

TABLE 1

Monitoring Index of Open-pit Mine

Monitoring category	Monitoring index	Description
Mine stope data	area	The total area of an open pit mine where mining is actually carried out
	volume	Total volume above the subbid price of the area where mining is actually carried out in an open pit mine
	Mining depth	Mining process, vertical distance from the surface to the lowest level of mining operation

5.2. TIN triangulation network is established

In this paper, the generated TIN triangulation network is used to obtain accurate stope index data of open pit. The mask of open pit stope extracted based on the improved Mine-YOLO model is applied to the DEM image to extract the elevation point set in this area, and the projection coordinates of corresponding elevation points are obtained by affine matrix. Based on the

obtained regional coordinate point set, Delaunay triangulation based on boundary constraints was performed to generate TIN triangulation network, which prepared the data for the subsequent automatic calculation of regional area, volume and mining depth. TIN triangulation generation process is shown in the following figure (Fig. 8). Delaunay triangulation is a classical triangulation method in computational geometry, which is mainly used to connect a set of discrete points into a non-overlapping triangular mesh. The generated triangle does not contain other points in the outer circle, and the inner circle radius is maximized as much as possible, so that the triangle shape is more regular and stable, the generated triangle minimum Angle is maximized, the triangle aspect ratio is reduced, and the mesh quality is improved. However, in general, the triangulation network will increase the subsequent area and volume. In order to make the triangulation network generated by the triangulation network more accurate in the subsequent calculation, boundary constraints are added to these discrete points [23]. The generation diagram is shown in the constraint-based triangulation process in Fig. 8

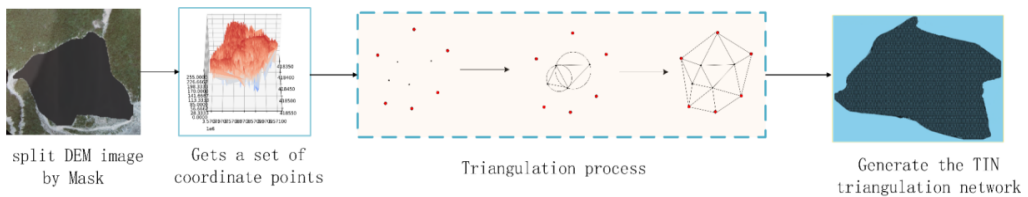


Fig. 8. Generate the TIN triangulation network

5.3. Calculation of maximum mining depth of slope

In open pit mining, slope depth is a key parameter, which is used to measure the mining depth of the deposit and the change of the surface during mining. The calculation of maximum mining depth is of great significance for mining planning, resource assessment and environmental impact assessment. Since the coordinate point set of slope area is known, the interpolation method is used to compare the current slope surface with the datum surface, and the mining depth is calculated through the elevation difference between the two, that is, the maximum mining depth value of the vertical distance from the lowest point to the surface in the slope area is calculated. The calculation algorithm is as follows:

$$h = H - \min(h_{list}) \quad (5)$$

Where H is the average surface elevation, h_{list} is the elevation array of the slope area, and \min is the algorithm for obtaining the minimum elevation in the slope area.

5.4. Slope surface area calculation

The Delaunay triangulation network consists of a series of triangles whose surface area is the sum of the areas of all triangles in the region. Arbitrary triangular three vertices A, B, C, three coordinates (x_A, y_A, z_A) , respectively (x_B, y_B, z_B) and (x_C, y_C, z_C) , trilateral side use of coordinate calculation.

Let the three sides be a , b and c . The calculation formula is as follows:

$$a = \sqrt{(x_B - x_C)^2 + (y_B - y_C)^2 + (z_B - z_C)^2} \quad (6)$$

$$b = \sqrt{(x_A - x_C)^2 + (y_A - y_C)^2 + (z_A - z_C)^2} \quad (7)$$

$$c = \sqrt{(x_B - x_A)^2 + (y_B - y_A)^2 + (z_B - z_A)^2} \quad (8)$$

Then its area according to Helen's formula is as follows:

$$S = \sqrt{p((p-a)(p-b)(p-c))} \quad (9)$$

Where $p = 1/2(a + b + c)$. The surface area of the Delaunay triangulation network is the sum of all triangle areas in the region as $S_{Surface}$:

$$S_{Surface} = \sum_{i=1}^n S_i \quad (10)$$

5.5. Stope volume calculation

Considering that the calculated mine volume elevation is always lower than the mining face, the volume of the space body is calculated using the following geometric volume calculation formula according to the spatial position relationship of the triangle. Triangular projection prism volume calculation:

$$V = \frac{S_{projection} z_A + z_B + z_C}{3} \quad (11)$$

Where $S_{projection}$ is the projected area of a triangle on the projection plane. By calculating the volume corresponding to a triangular mesh, you can add up the entire Delaunay triangulation volume as follows

$$V_t = \sum_{i=1}^n V_i \quad (12)$$

The projection calculation of the corresponding volume of a triangle in the TIN triangulation network is shown in the figure below (Fig. 9).

6. Experimental results and analysis

6.1. Experimental environment and training parameters

The experimental environment of this experiment is shown in the following table (TABLE 2). The improved YOLO model training was mainly completed under the server of the 64-bit Window 10 operating system.

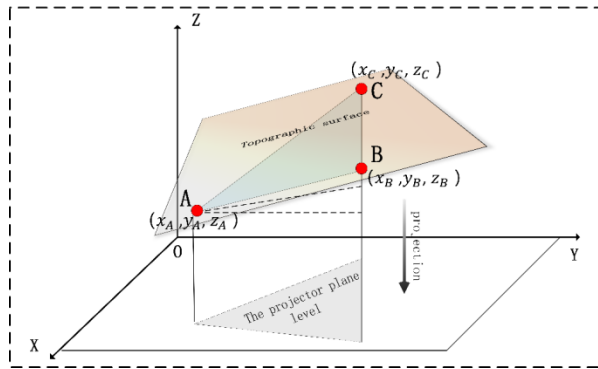


Fig. 9. TIN triangulation network volume calculation

TABLE 2

Experimental environment hardware and software configuration

Parameters	Configuration
CPU	Intel(R) Xeon(R) Gold 6348 2.59GHz
RAM	256 GB 3200 MHz
GPU	NVIDIA GeForce RTX 3090 24G
cuDNN	8.9.7
CUDA	12.4
Deep learning framework	Pytorch-2.2.1+python-3.9

In the experiment, a specially annotated surface mine image data set was used. The data set includes high-resolution aerial images of multiple stopes. In order to ensure the generalization ability of the model, the data set was randomly divided into training set (70%), verification set (20%) and test set (10%), and the number of model training iterations was set to 250 times. Specific experimental parameters are shown in the following table (TABLE 3).

TABLE 3

Experimental parameter setting

Parameters	Description	Configuration
Epochs	The number of training cycles	250
batch	The number of images per batch	10
imgsz	Enter the size of the image	640
workers	Number of worker threads for data loading	8
lr0	Initial learning rate	0.01
momentum	Learning momentum	0.937
box	Box loss gain	7.5
df1	Class loss gain	0.5
cls	df1 loss gain	1.2

6.2. Results and analysis of Mine-YOLO model

6.2.1. Model evaluation index

In order to verify the performance of the model in the two tasks of mining area, water body, vegetation restoration area and mining building segmentation and mine slope and collapse recognition, commonly used evaluation indicators for the two tasks were selected: Accuracy P_D and P_S , recall rate R_D and R_S , average accuracy mAP_D and mAP_S , where D is the evaluation index of target identification task and S is the evaluation index of segmentation task. The evaluation index formula is as follows:

$$P = \frac{TP}{TP + FP} \quad (13)$$

$$R = \frac{TP}{TP + FN} \quad (14)$$

$$mAP = \frac{1}{N} \sum_{i=1}^N AP_i \quad (15)$$

In the formula, TP represents the number of positive sample prediction correct, FN represents the number of positive sample prediction errors, and FP represents the number of negative sample prediction errors.

6.2.2. Model ablation experiment

In this paper, we systematically remove or modify the relevant modules of the model and study their effects on the performance of the model, which helps us to understand the importance of each part and its role. We took the standard YOLOv8n model as the baseline model, added each attention mechanism and loss function in the YOLO model, conducted experiments and recorded the performance results in target monitoring and semantic segmentation when the overlap threshold of the recognition box was 50%, as shown in TABLE 4. The training data has been explained above. It can be seen from the data that when no improvement module is included, the detection accuracy of 0.762 and the segmentation accuracy of 0.725 are relatively low. Only the addition of Focaler-IoU module has improved the accuracy, recall rate and average accuracy, indicating that Focaler-IoU module has effectively enhanced the model's ability to distinguish positive and negative samples, especially the improvement of detection accuracy from 0.762 to 0.777. The addition of only the EMA module significantly improves accuracy. The EMA module helps to improve the stability of the model, making it perform better when processing information. When only GAM module is added, the recall rates of detection and segmentation are 0.843 and 0.783 respectively, which are significantly improved, indicating that GAM module has a good effect on capturing global features and spatial information, especially in the recall rate. Combined with Focaler-IoU and EMA, the detection accuracy has been greatly improved, with the accuracy, recall rate and average accuracy reaching 0.838, 0.858 and 0.873, but the improvement in segmentation is not significant, indicating that the enhancement effect of these two modules on detection tasks is better than that of segmentation tasks. The combination of Focaler-IoU and GAM improves the detection accuracy, especially the segmentation accuracy, indicating that the combined use

of the two modules helps to improve the overall segmentation performance. The combination of EMA and GAM performed well on both detection and segmentation tasks with average detection and segmentation accuracy of 0.872 and 0.852, indicating that the combination of the two can complement each other in capturing global information and optimizing time series features, thereby improving the performance of the overall model. However, when all modules are added, the accuracy, recall rate, and average accuracy are 0.905, 0.863, and 0.942, and the segmentation accuracy, recall rate, and average accuracy are 0.842, 0.803, and 0.865. The synergy of all modules has greatly improved the performance of the model in all aspects, especially the accuracy of the detection task has been significantly improved. The analysis of experiments in each group shows that each module has a positive impact on the performance improvement of the model, Focaler-*IoU* is more inclined to improve the detection accuracy, EMA is helpful for the stability of the model and time series processing, and GAM is outstanding in the global feature capture. When all modules are combined, the model achieves the best performance, indicating that these modules can complement each other and jointly improve the overall performance of the model in surface mine stope data extraction.

TABLE 4

Comparison of ablation experiments of the models

Experiment	Focaler- <i>IoU</i>	EMA	GAM	P_D	R_D	$mAP_D@_{0.5}$	P_S	R_S	$mAP_S@_{0.5}$
1	×	×	×	0.762	0.685	0.792	0.725	0.754	0.786
2	√	×	×	0.777	0.698	0.833	0.753	0.783	0.818
3	×	√	×	0.789	0.817	0.858	0.764	0.797	0.834
4	×	×	√	0.783	0.843	0.824	0.783	0.743	0.783
5	√	√	×	0.838	0.858	0.873	0.778	0.793	0.815
6	√	×	√	0.816	0.843	0.838	0.753	0.828	0.788
7	×	√	√	0.844	0.858	0.872	0.821	0.797	0.852
8	√	√	√	0.905	0.863	0.942	0.842	0.803	0.865

6.2.3. Model comparison experiment

In order to further evaluate the recognition and segmentation performance of MINE-YOLO model in Mine stope, the experiment conducted a comparison experiment between MinE-YOLO model and other models of Mask R-CNN and YOLO series, and the experimental results were shown in TABLE 5. It can be seen from the table that model parameters are not direct factors affecting model

TABLE 5

Experimental Comparison of Different Models

Model	#param	P_D	R_D	$mAP_D@_{0.5}$	P_S	R_S	$mAP_S@_{0.5}$
YOLOv8n	3.1M	0.762	0.685	0.792	0.725	0.754	0.786
YOLOv8x	68.3M	0.845	0.732	0.811	0.823	0.785	0.804
YOLOv7n	36.5M	0.803	0.828	0.835	0.734	0.768	0.713
YOLOv5n	1.8M	0.688	0.754	0.653	0.618	0.647	0.638
YOLOv5x	86.8M	0.823	0.772	0.817	0.769	0.676	0.759
Mask R-CNN	42.5M	0.856	0.893	0.843	0.837	0.762	0.854
Mine-YOLO	46.5M	0.905	0.863	0.942	0.842	0.803	0.865

performance. Mine-YOLO and MaskR-CNN are smaller than YOLOv5x in terms of parameters, but the evaluation results show that the former model is much better than the latter. It can be seen that Mine-YOLO adds a spatial attention mechanism, which makes it have better recognition effect in complex and undulating terrain scenes such as mines. When the recognition box overlap threshold is 50%, the average accuracy of Mine-YOLO in target recognition reaches 0.942, and the average accuracy of Mine-YOLO in scene segmentation reaches 0.865. The model effect of YOLOv5n in the mine scene was poor, with the average accuracy of target recognition only 0.653 and the average accuracy of scene segmentation only 0.638. It can also be seen from the chart that Mask R-CNN performs well, and some related studies can be conducted based on Mask R-CNN in the future.

The Mine-YOLO model and other deep learning models were used to train and test the stope data set of open-pit mines. Part of the visualization results are shown in the figure below (Fig. 10). By comparing the reference value with the model recognition segmentation area, it can be seen that the Mine-YOLO model has a better recognition segmentation effect with less error extraction and missing extraction. In the processing of the boundary area, the improved YOLO model shows a higher detail capture ability and can clearly segment the complex stope boundary. In different terrain and environment, MinE-YOLO model shows high robustness and stability, and can adapt to various complex Mine terrain.

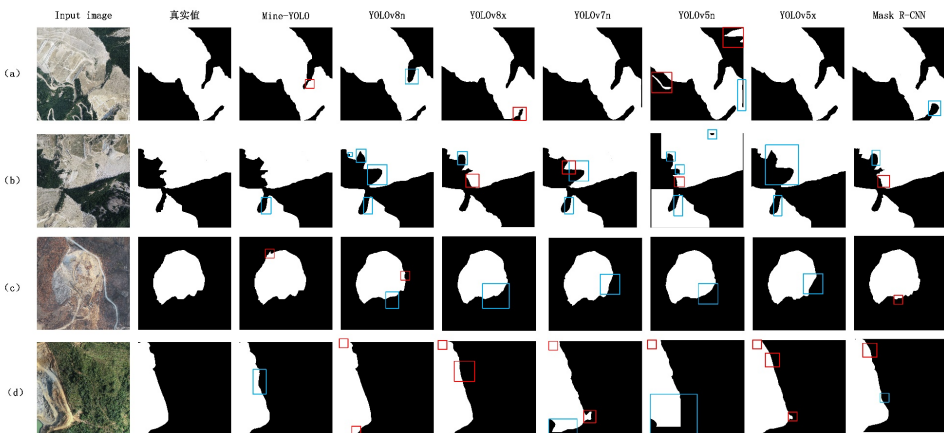


Fig. 10. Comparison of results of different models in identifying stope areas of open pit mines (The red mark is error extraction, and the blue mark is missing extraction)

6.3. Extraction results and analysis of stope information in open pit mine

As the data set of mining industry is strictly confidential, this paper obtains monitoring data of some mines based on the Xiangyang open-pit Mine dynamic monitoring project. In this section, the application effect of the improved Mine-YOLO model in open-pit mine monitoring is comprehensively displayed. The panoramic diagram of the applied mine is shown in Fig. 11. TIN triangulation network was established to obtain index data by extracting regions. These extraction results are shown in the table below (TABLE 6), indicating that the Mine-YOLO model proposed in this paper is feasible for monitoring open-pit mines.

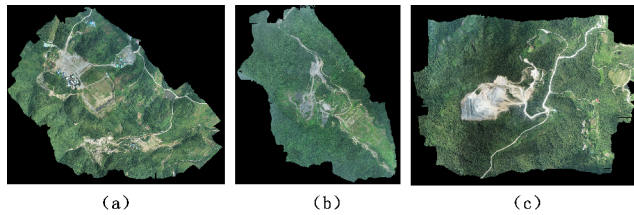


Fig. 11. Part of the monitoring mine panorama diagram. a. red tiled house; b. Longtan Ditch; c. Cow's tail

The following table (TABLE 6) shows the results obtained from the slope data of some open pit mines, and the slope data of three periods of the Mine are extracted, where E is the extracted value based on Mine-YOLO, and T is the calculated value based on the traditional ArcGIS of the mine. The error analysis diagram based on TABLE 6 (Fig. 12) shows that, based on the error analysis, The slope data obtained after the mining objects or scene targets extracted based on MinE-YOLO model have little difference with the traditional measured value. The average

TABLE 6

Results of Timing Extraction of Slope Information in Open-pit Mines

Mine	Date	Stope area /m ²		Stope volume /m ³		Mining depth /m	
		E	T	E	T	E	T
<i>a</i>	2022.08	479 454	466 253	14 990 096	14 506 500	212.5	212.2
	2023.08	489 230	467 800	12 022 578	12 453 500	203.6	203.4
	2023.12	485 322	469 287	11 890 552	11 003 600	197.2	197.2
<i>b</i>	2022.08	168 341	165 445	8 503 314	8 649 732	396.4	396.5
	2023.04	169 212	166 521	7 544 540	7 523 549	384.2	384.2
	2023.08	166 801	167 480	6 688 480	6 623 547	376.5	376.2
<i>c</i>	2022.08	253 208	211 018	11 566 816	9 978 245	109.5	110.3
	2023.04	228 319	215 514	9 983 984	9 768 521	101.5	100.4
	2023.08	248 341	221 842	9 864 360	9 088 532	93.9	93.9

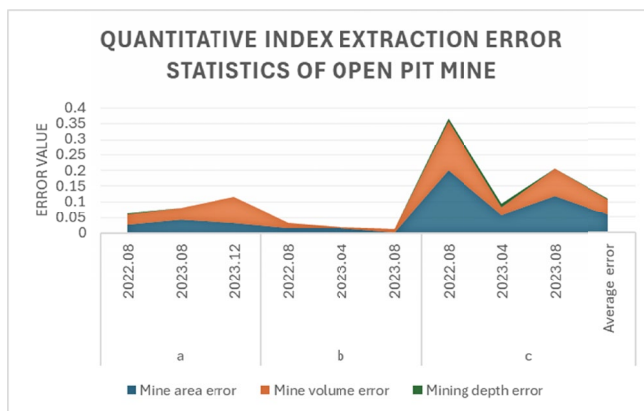


Fig. 12. Visualization of extraction error analysis of slope information index in some mines

error between area extraction and traditional measured value in open-pit Mine slope area is only 0.058, and the average error between volume extraction and traditional measured value is 0.049. The minimum monitoring error of mining depth index is 0.002. From the error analysis, it can be seen that the application of this method in practice is feasible.

7. Conclusion

This paper discusses the mining slope information extraction method based on Mine-YOLO, and specifically summarizes the contributions of this paper as follows:

- 1) An improved model Mine-YOLO is proposed, which adds the attention mechanism and replaces the lost Focaler-IoU function, so that the model is more sensitive to channel and spatial information and can obtain different levels of feature information, improving the recognition and extraction effect of the model in the complex scene of open-pit mines;
- 2) The target recognition accuracy of Mine-YOLO model in open pit mining reaches 0.905, the recall rate is 0.863, and the average accuracy is 0.942 when the recognition box overlap threshold is 50%. In the image segmentation task, the accuracy of the model is 0.842, the recall rate is 0.803, and the average accuracy is 0.865 when the recognition frame overlap threshold is 50%.
- 3) A method is proposed to accurately obtain quantitative monitoring data of mine area, volume and mining depth by using model to extract image area and generate TIN triangle network. Moreover, the method in this paper has high accuracy and small error in actually obtaining mine monitoring indicators. The average error of extracting area of mining area and volume of mining area is 0.058 and 0.047 respectively. The average error of extraction depth is 0.002.

To sum up, the Mine-YOLO model used in this paper can effectively provide technical support for slope identification and extraction in open pit mines. At the same time, triangulation network technology is used to achieve accurate acquisition of open-pit mine data, which provides the direction for realizing the accuracy, timing and dynamic automatic monitoring of open-pit mine.

Data availability statement

Data sets generated and analyzed in the course of the current study are available upon reasonable request by the corresponding author. These data cannot be disclosed due to government regulatory restrictions and competitive interests among companies.

References

- [1] Zh. Zhang, Y. Li, G. Nan, Exploration and practice of horizontal stratified mining in non-metallic open-pit mine in Hebei Province [J]. *China Mining Industry* **33** (06), 203-209 (2024). DOI: <https://doi.org/10.12075/j.j.issn.1004-4051.20240222>
- [2] R. Tombe, S. Viriri, Remote sensing image scene classification: Advances and open challenges [J]. *Geomatics* **3** (1), 137-155(2023). DOI: <https://doi.org/10.3390/geomatics3010007>
- [3] H. Ji, X. Luo, Implementation of Ensemble Deep Learning Coupled with Remote Sensing for the Quantitative Analysis of Changes in Arable Land Use in a Mining Area [J]. *Indian Soc Remote Sens.* **49**, 2875-2890 (2021). DOI: <https://doi.org/10.1007/s12524-021-01430-6>

- [4] J. Xiang, J. Chen, G. Sofia, et al., Open-pit mine geomorphic changes analysis using multi-temporal UAV survey [J]. *Environmental Earth Sciences* **77**, 1-18 (2018). DOI: <https://doi.org/10.1007/s12665-018-7383-9>
- [5] C.H. Lin, T.Y. Wang, A novel convolutional neural network architecture of multispectral remote sensing images for automatic material classification [J]. *Signal Processing Image Communication* **97** (105), 116329 (2021). DOI: <https://doi.org/10.1016/j.image.2021.116329>
- [6] W. Zhang, P. Tang, L. Zhao, Remote Sensing Image Scene Classification Using CNN-CapsNet [J]. *Remote Sensing* **11** (5), 494 (2019). DOI: <https://doi.org/10.3390/rs11050494>
- [7] Y. Liu, Y. Zhong, F. Fei, et al., Scene semantic classification based on random-scale stretched convolutional neural network for high-spatial resolution remote sensing imagery [C]. 2016 IEEE International Geoscience and Remote Sensing Symposium (IGARSS). IEEE **2016**, 763-766 (2016). DOI: <https://doi.org/10.1109/igarss.2016.7729192>
- [8] R. Balaniuk, O. Isupova, S. Reece, Mining and tailings dam detection in satellite imagery using deep learning [J]. *Sensors* **20** (23), 6936 (2020). DOI: <https://doi.org/10.3390/s20236936>
- [9] H. Xie, Y. Pan, J. Luan, et al., Semantic segmentation of open pit mining area based on remote sensing shallow features and deep learning [C]. Big Data Analytics for Cyber-Physical System in Smart City: BDCPS 2020, 28-29 December 2020, Shanghai, China. Springer Singapore **2021**, 52-59 (2021). DOI: https://doi.org/10.1007/978-981-33-4572-0_8
- [10] T. Chen, X. Zheng, R. Niu, et al., Open-pit mine area map with Gaofen-2 satellite images using U-Net+ [J]. *IEEE Journal of Selected Topics in Applied Earth Observations and Remote Sensing* **15**, 3589-3599 (2022). DOI: <https://doi.org/10.1109/jstars.2022.3171290>
- [11] H. Xie, Y. Pan, J. Luan, et al., Open-pit mining area segmentation of remote sensing images based on DUsegNet [J]. *Journal of the Indian Society of Remote Sensing* **49** (6), 1257-1270 (2021). DOI: <https://doi.org/10.1007/s12524-021-01312-x>
- [12] Y. Liu, C. Li, J. Huang, et al. MineSDS: A Unified Framework for Small Object Detection and Drivable Area Segmentation for Open-Pit Mining Scenario [J]. *Sensors* **23** (13), 5977 (2023). DOI: <https://doi.org/10.3390/s23135977>
- [13] X. Meng, D. Zhang, S. Dong, C. Yao, Open-Pit Granite Mining Area Extraction Using UAV Aerial Images and the Novel GIPNet. *Remote Sensing* **16** (5), 789 (2024). DOI: <https://doi.org/10.3390/rs16050789>
- [14] D. Guo, Y. Zhang, Image detection of coal gangue based on lightweight PAM-M-YOLO model [J]. *Mining Research and Development* **44** (5), 220-227 (2018).
- [15] Sh. Ruan, Sh. Yan, Q. Gu, et al., Road negative obstacle detection in open pit mining area based on multi-feature fusion [J]. *Journal of China Coal Society* **49** (5), 2561-2572 (2019). DOI: <https://doi.org/10.13225/j.cnki.jccs.2023.0539>
- [16] Y. Liu, Z. Shao, N. Hoffmann, Global attention mechanism: Retain information to enhance channel-spatial interactions [J]. arXiv preprint arXiv: 2112, 05561 (2021). DOI: <https://doi.org/10.48550/arXiv.2112.05561>
- [17] W. Hao, C. Ren, M. Han, et al., Cattle body detection based on YOLOv5-EMA for precision livestock farming [J]. *Animals* **13** (22) 3535 (2023). DOI: <https://doi.org/10.3390/ani13223535>
- [18] Z. Ren, L. Wang, Z. He, Open-Pit Mining Area Extraction from High-Resolution Remote Sensing Images Based on EMANet and FC-CRF. *Remote Sensing* **15** (15), 3829 (2023). DOI: <https://doi.org/10.3390/rs15153829>
- [19] H. Zhang, S. Zhang, Focaler-IoU: More Focused Intersection over Union Loss [J]. arXiv preprint arXiv: 2401, 10525 (2024). DOI: <https://doi.org/10.48550/arXiv.2401.10525>
- [20] H. Jiale, Zh. Min, Sh. Fei, RTDETR improvement for unmanned aerial vehicle (uav) small target detection algorithm [J/OL]. *Computer Engineering and Application* 1-11 (2024). <http://kns.cnki.net/kcms/detail/11.2127.TP.20240624.1520.010.html>. DOI: 10.3778/j.issn.1002-8331.2404-0114
- [21] L. Yi, Z. Huang, Y. Yi, Improved YOLOv8 foreign body detection method of transmission lines [J/OL]. *Electronic Measurement Technology*, 1-11 (2024). <http://kns.cnki.net/kcms/detail/11.2175.TN.20240927.1427.138.html>
- [22] D. Li, G. Wang, Y. Guo, et al., Image recognition method of coal waste in complex working environment based on CFS-YOLO algorithm [J]. *Coal Science and Technology* **52** (6), 226-237 (2018). DOI: <https://doi.org/10.12438/cst.2023-1967>
- [23] X. Tan, B. Zhu, J. Wang, et al., An efficient improved TIN growth algorithm for discrete elevation points [J]. *Journal of Naval University of Engineering* **35** (02), 25-30 (2023).